Evolution of short-range magnetic correlations in ferromagnetic Ni-V alloys

Shiva Bhattarai,[1] Hind Adawi [ORCID],[1,2] Jean-Guy Lussier [ORCID],[1] Adane Gebretsadik [ORCID],[1,*] Maxim Dzero,[1]
Kathryn L. Krycka [ORCID],[3] and Almut Schroeder [ORCID][1,†]

[1]*Physics Department, Kent State University, Kent, Ohio 44242, USA*
[2]*Department of Physics, Jazan University, Jazan 45142, Kingdom of Saudi Arabia*
[3]*NIST Center for Neutron Research, National Institute of Standards and Technology, Gaithersburg, Maryland 20899, USA*

We experimentally study how the magnetic correlations develop in a binary alloy close to the ferromagnetic quantum critical point with small-angle neutron scattering (SANS). Upon alloying the itinerant ferromagnet nickel with vanadium, the ferromagnetic order is continuously suppressed. The critical temperature T_c vanishes when vanadium concentrations reach the critical value of $x_c = 0.116$ indicating a quantum critical point separating the ferromagnetic and paramagnetic phases. Earlier magnetization and μSR data have indicated the presence of magnetic inhomogeneities in $Ni_{1-x}V_x$ and, in particular, recognize the magnetic clusters close to x_c, on the paramagnetic and on the ferromagnetic sides with nontrivial dynamical properties [R. Wang *et al.*, Phys. Rev. Lett. **118**, 267202 (2017)]. We present the results of SANS study with full polarization analysis of polycrystalline $Ni_{1-x}V_x$ samples with $x = 0.10$ and $x = 0.11$ with low critical temperatures $T_c < 50$ K. For both Ni-V samples close to x_c we find isotropic magnetic short-range correlations on the nanometer scale persisting at low temperatures. They are suppressed gradually in higher magnetic fields. In addition, signatures of long-range ordered magnetic domains are present below T_c. The fraction of these magnetic clusters embedded in the ferromagnetic ordered phase grows toward x_c and agrees well with the cluster fraction estimate from the magnetization and μSR data. Our SANS studies provide new insights into the nature of the inhomogeneities in a ferromagnetic alloy close to a quantum critical point.

I. INTRODUCTION

Ferromagnetic order emerging as a result of electron-electron interactions in metals has been studied extensively during the last several decades. In clean metals if the spin-exchange interactions between the itinerant electrons are strong enough, then the ferromagnetic order develops at some finite temperature [1–3]. For example, for Ni the critical temperature of the ferromagnetic transition is $T_c \approx 630$ K. Introduction of disorder by alloying is a way to suppress the ferromagnetic transition, so that the critical temperature becomes zero at some finite concentration of impurity atoms x_c. For example, in $Ni_{1-x}V_x$ alloys the critical concentration is $x_c \approx 0.116$ [4].

When $x = x_c$ a quantum phase transition (QPT) between the ferromagnetic and paramagnetic states is expected to occur. Since the symmetry of the ground state changes at the quantum critical point (QCP), the evolving quantum critical fluctuations affect the vicinity of the QCP, including finite temperatures that lead to unusual thermal properties [5]. Since the transition is driven by spin-exchange interactions, which for each realization of disorder become nonlocal and random, QPTs are expected to be affected by disorder more likely than thermal phase transitions [6].

Under the proper conditions random quenched disorder in a metallic system can produce a quantum Griffiths phase [7,8] that is usually recognized by anomalous thermodynamic properties [8] close to the QCP. In this case, a distribution of magnetic fluctuations with different timescales including very slow rare regions [7] dominates the magnetic response. Specifically, experimental signatures of the Griffiths phase are power laws with nonuniversal exponents [9] in thermodynamic responses. These power laws are observed in many systems [4,10], but the responsible fluctuations with different time and and length scales have not been demonstrated directly. In general, disordered alloys close to a ferromagnetic QCP are recognized by unusual scaling behavior [11–13]. Specific effective exponents are predicted for disordered FMs [14,15]. Note that QCPs in FMs are rare; more often new phases emerge when T_c gets suppressed [15]. Typically, clean FMs rather present a first-order transition [15] without critical fluctuations. So remarkably, introducing disorder is a unique route for a QCP in itinerant FMs such as Ni. The characterization of the critical fluctuation spectrum should reveal the nature of this special point.

Lastly, we note that the conclusion that only disorder allows to the QCP in itinerant ferromagnets is a simplification as alternative mechanisms have been recently proposed to explain a ferromagnetic QCP [16] with critical fluctuations. For example, the experimental signatures of the quantum critical fluctuations were reported in chemically tuned Ni-Rh [17] and pressure-tuned $CeRh_6Ge_4$ [18,19] from ferromagnetic systems where disorder is considered negligible.

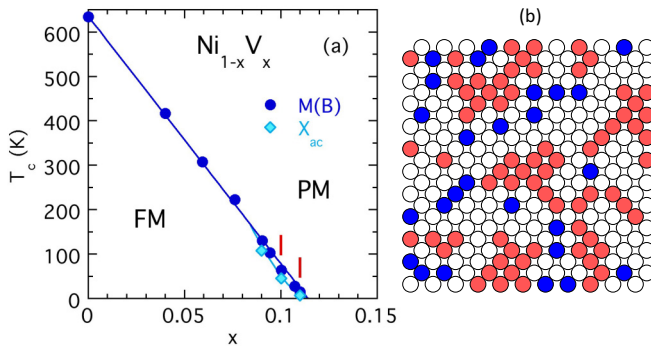*Present address: Intel, Chandler, Arizona, USA.
†aschroe2@kent.edu

FIG. 1. (a) Magnetic phase diagram of $Ni_{1-x}V_x$ displaying the critical temperature T_c vs vanadium concentration x separating the ferromagnetic ordered phase (FM) from the paramagnetic phase (PM) leading to a quantum critical point [26]. The red markers indicate the samples for this investigation. The right panel (b) demonstrates the magnetic inhomogeneities in $Ni_{1-x}V_x$ with $x = 0.10$ in an fcc lattice plane: it shows how randomly placed V atoms (in blue) separate Ni-rich regions (in red) responsible for magnetism. Since V affects more the moment of the local Ni neighbors, we distinguish these close Ni sites (in white) from the rest, the more distant Ni atoms (in red).

As we have mentioned above, $Ni_{1-x}V_x$ is an example of a disordered metallic system which exhibits the signatures of a ferromagnetic QCP indicating the presence of quantum critical fluctuations. In this paper, we present the results of the measurements which directly probe quantum critical magnetic fluctuations in the vicinity of the ferromagnetic QPT driven by disorder. In particular, we use small-angle neutron scattering (SANS) to probe the magnetic microstructure and magnetic inhomogeneity on the mesoscopic length scale of interest from a few to a hundred nanometers [20]. We are motivated by the fact that SANS successfully revealed the correlation length change of critical fluctuations close to a phase transition in several magnetic alloys [21–25]. We present the experimental evidence of magnetic correlations at various length scales in a ferromagnetic Ni alloy introduced by random atomic substitution of Ni by V. These findings are compatible with a quantum Griffiths phase.

II. EXPERIMENTAL METHODS

A. Ni-V

The alloys of $Ni_{1-x}V_x$ provide a good platform to study a random disordered QPT not only because of their low magnetic anisotropy and the "large defects" caused by vanadium, but also because they form indeed good solid solutions with random atomic disorder. In addition, when the vanadium concentration reaches the value of $x_c = 0.116$ these binary alloys exhibit a quantum phase transition (QPT) from the ferromagnetic (FM) to the paramagnetic (PM) phase with a quantum critical point (QCP) [4]. Figure 1(a) shows the phase diagram. It is known that V affects the electronic state of the Ni neighbors and causes therefore large magnetic inhomogeneities [27] and an effective reduction of the magnetic moment with low x_c [28]. In Fig. 1(b) we present a schematic view of a lattice plane with V on random lattice sites. Assuming that V

causes a moment reduction of neighboring Ni, the undisturbed magnetic Ni network becomes inhomogeneous.

Previous studies reveal some signatures of a quantum Griffiths phase. Specifically, for $x \approx x_c$ the magnetization data $M(B)$ show the nonuniversal power law dependencies [4,26]. This is further supported by μSR data recognizing a field distribution in the samples [29], and the ferromagnetic alloys with values of x close to x_c include a dynamic contribution to $M(B)$ besides the static contribution [26].

All samples keep the simple fcc crystal structure. The polycrystalline samples were arc-melted and annealed at high temperatures and cooled down fast to maintain the random atomic placement of the V on the fcc lattice sites at low temperatures. A structural study (PDF analysis from wide-angle neutron diffraction data [26,30]) confirmed the random atomic distribution of V and the otherwise unchanged crystalline fcc lattice at low temperatures.

B. Experimental details

We use the same polycrystalline samples prepared for optimized random atomic distribution as studied before by different methods [4,26,30]. For the small-angle neutron scattering (SANS) study we chose the concentrations $x = 0.10$, $x = 0.11$, and $x = 0$. The samples with $x = 0.11$ are made with ^{58}Ni, while the others contain natural Ni isotope mixtures, which yield different nuclear neutron cross sections of Ni. The SANS experiments were performed at the instruments NG7SANS [31] and VSANS [32], at the NIST Center for Neutron Research (NCNR) at the National Institute of Standards and Technology and at the instrument GPSANS, at the high-flux isotope reactor (HFIR) at Oak Ridge National Laboratory. We focus here most on the SANS experiments that allow a full polarization analysis from NG7SANS. Several 3 mm diameter pellets of each concentration were wrapped in Al foil and placed on a Cd-mask framed Al-sample holder attached to the cold plate of the cryostat. To cover a wave vector range of $Q = (0.06–1)$ nm^{-1} with neutron wavelengths of 0.55 nm and 0.75 nm, the SANS intensity was collected in the xy plane on a 2D detector at different samples to detector distances (from 2 m to 11 m). We obtained the different polarized cross sections, e.g. the non-spin-flip (NSF) scattering with unchanged polarization state of the neutrons (DD and UU) and spin-flip (SF) scattering with reverse polarization state (DU and UD) from the sample, using the supermirror polarizer and ^{3}He cell as a spin analyzer as stated in detail in Refs. [33,34]. See setup in Fig. 2. U, D refer to the up, down aligned neutron spins with regard to the axis of neutron polarization determined by the external magnetic field. The magnetic field was applied in the x direction ($B_{min} = 7$ mT, $B_{max} = 1.5$ T) perpendicular to the beam ($\parallel z$). θ indicates the azimuthal angle within the xy plane, with $\theta = 0°$ in the horizontal x direction and $\theta = 90°$ in vertical y direction of the detector. Most of the data were reduced and analyzed with the IGOR software [35].

C. Polarized SANS analysis

The fully polarized SANS (PASANS) technique traces the neutron spin before it enters and after it leaves the sample
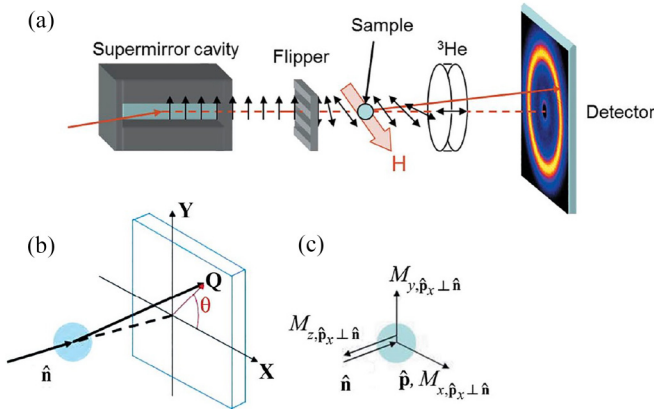
FIG. 2. (a) Polarized SANS setup with polarizing supermirror, spin flipper, sample in a cryostat with a magnetic field perpendicular to the neutron beam, a ^{3}He analyzer, and a position-sensitive detector. Arrows indicate neutron polarization direction. (b) Coordinate axes with beam direction $\hat{n}$ along z defining angle θ in the xy plane of the detector. (c) Present setup of field and polarization direction $\hat{p}$ along x (from Ref. [36]).

separately. The four different cross sections (DD, UU, DU, UD) offer the advantage of separating the small magnetic scattering from overwhelming nuclear scattering in our samples [37]. Here we use in particular the angle dependence [36] of the signal in the xy plane of the detector to resolve magnetic components M_x^2, M_y^2, M_z^2, with a magnetic field B_x perpendicular to the beam. We apply two methods to best trace the magnetic signal. First we collect the pure SF signal (DU + UD) that ideally selects "magnetic" scattering. But it contains other "background" (BG) contributions due to incoherent scattering from the sample and other sources. A small SF contribution of V nuclear spins is also included that does not show any angle dependence [37,38].

The NSF signal (DD + UU) is only used in limited cases to extract some strong longitudinal component M_x^2 when the nuclear contribution N^2 and its sample variation are not dominating. Otherwise, we use the flipper contrast of NSF data called DIF of fully polarized (DD-UU) or half-polarized data (D-U) to recognize the anisotropic M_x component of the mixed term $2NM_x$ that contains a strong nuclear contribution. For our geometry we do not expect and do not see any indication of anisotropy in the transverse direction of the field, so that we keep $M_y = M_z = 0$, while $M_x > 0$.

Note that the intensity shown is not calibrated; it is consistent for each sample. Different number and size of pellets and the different cross sections of ^{58}Ni and of natural Ni lead to different responses for both samples with $x = 0.11$ and $x = 0.10$, respectively. We omit also any proportionality factor in the equation (more details and general forms are given in Ref. [36]).

The angular dependence for the SF response is therefore

$$\mathrm{SF}(\theta) = M_z^2 + M_y^2 \cos^4 \theta + M_x^2 \cos^2 \theta \sin^2 \theta + \mathrm{BG_{SF}}. \quad (1)$$

For the case of isotropic magnetic correlations where $M_x^2 = M_y^2 = M_z^2 = \frac{1}{3}M_{\mathrm{tot}}^2$, we expect a simple cosine-square

response with amplitude of $\frac{1}{3}M_{\mathrm{tot}}^2$:

$$\mathrm{SF}(\theta) = M_y^2(1 + \cos^2 \theta) + \mathrm{BG_{SF}}. \quad (2)$$

In particular, the SF contrast, the difference between SF data in a horizontal sector ($\theta = 0°$ and $180°$) called SFH and a vertical sector ($\theta = \pm 90°$) called SFV, each collected typically within $\delta \pm 30°$, produces the transverse component M_y^2 without any $\mathrm{BG_{SF}}$. Ideally $\mathrm{BG_{SF}}$ cancels out in the difference assuming the other contributions to $\mathrm{SF}(\theta)$ are not angle dependent:

$$\mathrm{SF}(\theta = 0°) - \mathrm{SF}(\theta = 90°) = M_y^2(Q). \quad (3)$$

This SF contrast can be evaluated over the accessible Q regime to study the magnetic correlation lengths.

In principle the total non-spin-flip data NSF serve to extract the longitudinal component of the magnetic scattering, M_x^2, from the angular dependence. But the extra constant is not small and not angle-independent due to the nonhomogeneous sample arrangement. The nuclear scattering of the sample N^2 dominates typically the response compared to other external BG and magnetic signals,

$$\mathrm{NSF_{tot}}(\theta) = N^2 + M_x^2 \sin^4 \theta + M_y^2 \cos^2 \theta \sin^2 \theta + \mathrm{BG_{NSF}}. \quad (4)$$

For isotropic correlations we get a simple sine-square variation with amplitude $M_x^2 = \frac{1}{3}M_{\mathrm{tot}}^2$:

$$\mathrm{NSF}(\theta) = N^2 + M_x^2 \sin^2 \theta + \mathrm{BG_{NSF}}. \quad (5)$$

The different response between the two polarization directions (without registering spin flip), the NSF asymmetry or DIF (DD-UU or D-U), yields an interference term of nuclear and magnetic origin. It signals a weak contribution from a center with a net magnetic component along the x direction M_x in the presence of a strong nuclear contribution from the same center:

$$\mathrm{DIF}(\theta) = 2NM_x \sin^2 \theta. \quad (6)$$

The vertical sector cut DIFV (collected at $\theta = \pm 90°$ within $\delta \pm 30°$) gives the maximum signal $2NM_x$. We can trace this DIFV term over a large Q regime resolving an anisotropic magnetic response M_x from 0.06 nm^{-1} to 1 nm^{-1} in the Ni$_{1-x}$V$_x$ samples.

III. RESULTS OF SANS STUDY

We collected indications of disorder and clusters in Ni$_{1-x}$V$_x$ alloys [26] related to a quantum Griffith phase. But any information of length and time scales of these unusual magnetic clusters is still lacking. Initial SANS experiments demonstrated that some magnetic signal can be detected for samples with small vanadium concentration $x < x_c$, while the magnetic intensity in the paramagnetic regime ($x > x_c$) seems too small to be noticed with an averaged high-field magnetic moment of less than 0.01 μ_B/atom [4]. More recent (unpolarized) SANS data collected at GPSANS show promising temperature and field dependent signals, and finally polarized SANS data can identify consistently a magnetic response. Some data with preliminary analysis for the compound Ni$_{0.9}$V$_{0.10}$ with the higher critical temperature $T_c \approx$

50 K are shown in Ref. [38]. Here we present the PASANS results of the samples closest to the critical point with the lowest T_c in contrast to pure Ni. We show in detail the magnetic responses of $Ni_{0.89}V_{0.11}$ with $T_c = 7$ K and compare them with $Ni_{0.9}V_{0.10}$ with $T_c \approx 50$ K to figure out the relevant magnetic correlations, their correlation length, and their evolution toward x_c.

A. Short-range correlations in $Ni_{0.90}V_{0.10}$

The first challenge is to extract the small magnetic scattering from the large nuclear contribution of Ni. The background of "nonmagnetic scattering" is high because of the high nuclear cross section of Ni compared to the small magnetic cross section due to the reduced average magnetic moment (<0.1 μ_B/Ni) in these alloys. The additional grain boundary scattering observed in our polycrystalline samples dominates toward lower scattering vectors Q. We use the (azimuthal) angle dependence (in the xy plane of the detector) of selected cross sections to resolve the magnetic components M_x^2, M_y^2, M_z^2 with a magnetic field B_x perpendicular to the beam (along z). Section II C presents the relevant expressions for our setup shown in Figs. 2(b) and 2(c).

First, we focus on the spin-flip (SF) signal to recognize the magnetic scattering. The angle dependence of SF(θ) as predicted by Eq. (1) further separates magnetic scattering from the background contribution and recognizes spin anisotropies. We distinguish a longitudinal magnetic component M_x^2 from transverse magnetic components M_y^2 and M_z^2 (with a wave vector Q perpendicular to z). Figure 3 presents SF(θ) and the non-spin-flip signal NSF(θ) of $Ni_{0.9}V_{0.10}$ in a medium Q range (0.45 ± 0.15) nm^{-1}. Both show significant variations in the angle θ most obvious for a temperature close to T_c, which signals a magnetic response according to Eqs. (1) and (4). The fit looks even like a simple cosine-square function for SF(θ) and a sine-square for NSF(θ) with the same amplitude, which signals $M_y^2 = M_z^2$ [see Eqs. (2) and (5)]. The fit parameters M_y^2 and M_x^2 evaluated at a specific Q range from SF(θ) and NSF(θ) are presented in Fig. 4 for different temperatures and fields. It is obvious in the left panels (a) and (b) that both the transverse M_y^2 and longitudinal M_x^2 components are the same at T_c and stay the same for all T in small fields.

For low fields (of 7 mT) the magnetic response is isotropic in this medium Q regime for high temperatures $T > T_c$ like expected in the PM regime. The signal is strongest at the critical temperature T_c and decreases for temperatures above and below T_c as seen in Fig. 3 and Fig. 4. Note that at the lowest temperature, $T = 3$ K, the magnetic signal does not completely vanish. In the FM regime below T_c we need to apply a slightly higher field of 50 mT to keep the neutron beam sufficiently polarized with $P_S > 85\%$ for a polarization analysis (see Appendix). In this small field of 50 mT the response looks still isotropic. The simple cosine-square or sine-square form with reduced but finite amplitude indicates that isotropic magnetic fluctuations remain in the FM state as observed in the PM state. These magnetic fluctuations change in higher magnetic fields. The M_y^2 component in the SF response is reduced while the longitudinal component M_x^2 seems less affected. The M_x^2 component is more difficult to
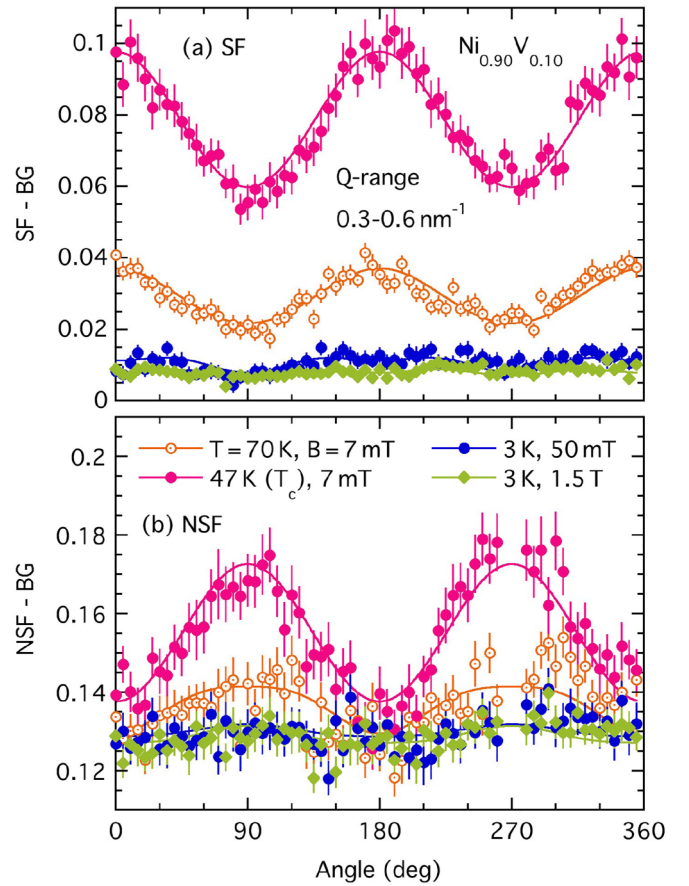

FIG. 3. Neutron scattering intensity of $Ni_{0.90}V_{0.10}$ vs azimuthal angle θ collected in medium Q range of $(0.3–0.6)$ nm^{-1} at different temperatures T and magnetic fields B. The upper panel (a) presents the SF data, the lower panel (b) the NSF data with fit as solid line using Eq. (1) in (a) and Eq. (4) in (b). An angle-independent background BG has been subtracted from the data, which varies with spin filter and B.

determine; it is a small disturbance to the SF(θ) shape or is the main parameter from the NSF(θ) data that include a high nuclear response. Through these angle-dependent data we are able to confirm magnetic scattering at finite Q in $Ni_{0.90}V_{0.10}$ at low T. Since they display the same isotropy as in the PM state, it is likely that they are fluctuations with sufficiently long timescales to be observed as static by the neutrons. This magnetic signal looks promising to uncover the "magnetic clusters," the distribution of clusters with different sizes and fluctuation rates that evolve at a disordered QCP.

The Q dependence of SANS reveals some direct information about the relevant magnetic correlation length of these clusters. Figure 5 displays the Q dependence of the SF signal, i.e., the M_y^2 component from the SF contrast (SFH-SFV). Since the signal is isotropic (in low fields) M_y^2 represents $1/3$ of the total magnetic signal M_{tot}^2. M_y^2 can be resolved in a limited Q range above 0.1 nm^{-1}. Toward lower Q, the dominating nuclear NSF contribution increases and makes the extraction of a small SF contribution with polarization corrections less reliable. The even smaller SF contrast cannot be resolved. The strongest response is found at 47 K close
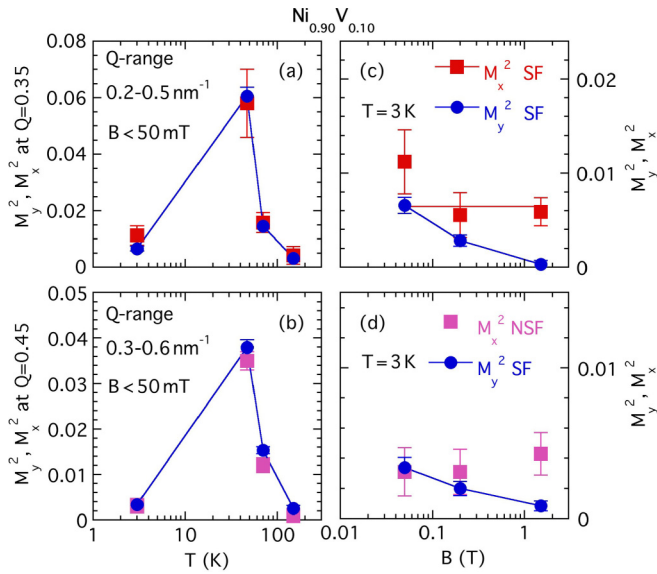
FIG. 4. Temperature T and magnetic field B dependence of magnetic transverse components M_y^2 and longitudinal component M_x^2 of $Ni_{0.90}V_{0.10}$. In the upper panel [(a), (c)] M_y^2 and M_x^2 are extracted from fit [Eq. (1)] of $SF(\theta)$ at Q range $(0.2–0.5)$ nm^{-1}. The lower panel [(b), (d)] presents the main components from the data shown in Fig. 3 at Q range $(0.3–0.6)$ nm^{-1}: M_y^2 comes from fit of $SF(\theta)$ and M_x^2 from fit [Eq. (4)] of $NSF(\theta)$.

to T_c. M_y^2 is clearly Q-dependent, steeper at T_c than at higher temperatures $T = 70$ K. At the lowest temperature of $T = 3$ K $M_y^2(Q)$ can be barely resolved beyond the middle-Q region but its Q dependence looks similar to the $T = 47$ K data. Within this limited Q region of $(0.1–1)$ nm^{-1} the SF contrast can be approximated well by a Lorentzian function as expected for paramagnetic critical scattering of the Ornstein-Zernike form with a correlation length $\xi = 1/\kappa$:
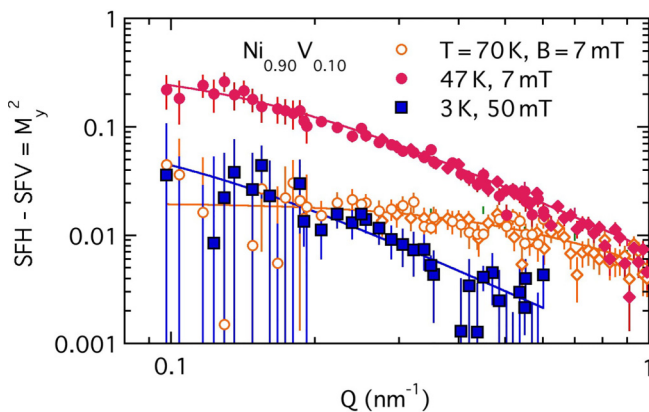
$$M_y^2 = A_L \times \kappa^2/(\kappa^2 + Q^2). \tag{7}$$

FIG. 5. Magnetic neutron scattering intensity vs wave vector Q for $Ni_{0.90}V_{0.10}$. The spin-flip contrast SFH-SFV is shown in small magnetic fields ($B \leqslant 50$ mT) representing M_y^2 or $1/3$ of the total isotropic magnetic response M_{tot}^2 for different temperatures T. Solid lines are Lorentzian fits using Eq. (7).

We estimate a correlation length using Eq. (7) as $\xi \approx (7 \pm 2)$ nm for $T \approx T_c = 47$ K, and we find the comparable value of $\xi = (10 \pm 6)$ nm in a more restricted Q regime for $T = 3$ K. About 10% of the amplitude A_L of the Lorentzian form remains at low T: $A_L(T = 3$ K$) \approx (1/10)A_L(T = 47$ K$)$. That corresponds to the same fraction of M_y^2 at medium Q. These data clearly show some leftover short-range magnetic correlations in the FM state at $T < T_c$ that do not contribute to the long-range order. The remaining magnetic response at low temperatures is similar to the PM scattering. The cluster sizes or range of correlation length at low T look like those estimates in the PM regime close to T_c. The nonpolarized data estimates for $x = 0.10$ using high-field data as reference agree with the main PASANS findings [38].

B. Short-range correlations in $Ni_{0.89}V_{0.11}$

The discovery of a remaining magnetic signal in $Ni_{0.90}V_{0.10}$ motivates us to investigate the more diluted $Ni_{0.89}V_{0.11}$ that is closer to critical concentration x_c with a lower $T_c = 7$ K. As expected the magnetic response in $Ni_{0.89}V_{0.11}$ is even smaller than in $Ni_{0.90}V_{0.10}$ and more challenging to resolve. Note that the data shown are not calibrated and a direct comparison of the scattering intensities of $x = 0.11$ and $x = 0.10$ cannot be made. We cannot extract any clear magnetic signal from the NSF data due to the strong nuclear contribution in $x = 0.11$. But the SF data reveal successfully a magnetic response from the distinct angle dependence in a limited Q regime. The strongest SF response in $Ni_{0.89}V_{0.11}$ close to T_c at $T = 8$ K follows a simple cosine-square function as seen in Fig. 6(a). All $SF(Q)$ data can be described well by Eq. (1) confirming an isotropic magnetic response with $M_y^2 = M_x^2$ in low fields ($B \leqslant 50$ mT). The T dependence of these transverse and longitudinal components is shown in Fig. 8(a). Similarly to $Ni_{0.90}V_{0.10}$ the strongest PM response of fluctuating short-range correlations develops upon cooling toward T_c, decays for $T < T_c$, but does not vanish for the lowest T. Also the Q dependence of the SF contrast (SFH-SFV) that measures the transverse component M_y^2 of the isotropic fluctuations looks similar for both concentrations as displayed in Figs. 5 and 7. For $Ni_{0.89}V_{0.11}$ the Q range and precision of the data are more limited. $M_y^2(Q)$ can be described by a Lorentzian line shape with Eq. (7). Cooling toward T_c increases the correlation length $\xi = 1/\kappa$, but it remains finite at T_c. $M_y^2(Q)$ shows about the same Q dependence at the lowest T of 4 K compared to T_c. Only the amplitude A_L is reduced. Fitting the SF contrast at 8 K and 4 K including data up to 1 nm^{-1} (not all data shown) yields $\xi = (4 \pm 2)$ nm and $\xi = (6 \pm 3)$ nm, respectively. Within this large uncertainty we conclude that the typical correlation length at T_c and at low T is quite similar in the range of 5–10 nm and not very distinct from $Ni_{0.90}V_{0.10}$. These simple estimates show some indication that the magnetic length scale describing the cluster distribution might become smaller toward the critical point, but only better precision estimates from a larger Q regime with improved statistics of the low intensity $x = 0.11$ data can clarify that. Most importantly, these polarized data are able to confirm that magnetic clusters are still present at low T, which look similar to PM scattering with a typical scale of a few nm. In $Ni_{0.89}V_{0.11}$ the magnetic cluster response M_y^2
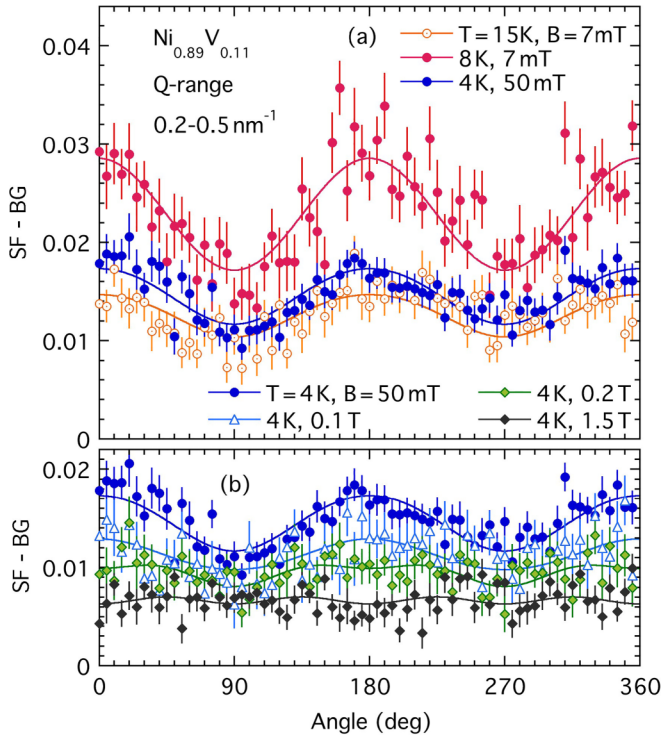
FIG. 6. Angle dependence of SF signal collected in medium Q range (0.35 ± 0.15) nm^{-1} for Ni$_{0.89}$V$_{0.11}$. Panel (a) shows data in small magnetic fields B at different temperatures T, and panel (b) data at low T in different B. Fit is shown as solid line using Eq. (1). A constant BG has been subtracted from the data that depends on polarization filter and magnetic field.

at 4 K is about half of M_y^2 at T_c for this medium Q range. While the remaining cluster contribution is about of similar magnitude in both samples, the fraction of remaining clusters is much higher in $x = 0.11$ than in $x = 0.10$. The present data (not shown in the same scale) do not allow us to trace a detailed concentration dependence of the remaining clusters.
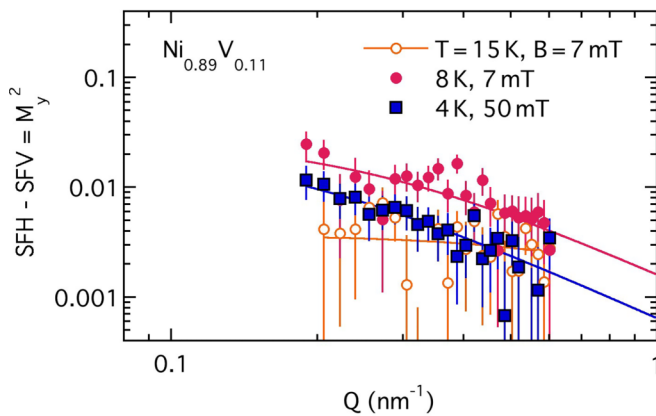

FIG. 7. Magnetic neutron scattering intensity vs wave vector Q for Ni$_{0.89}$V$_{0.11}$. The spin-flip contrast SFH-SFV is shown in small magnetic fields $(B \leqslant 50$ mT) representing M_y^2 or $1/3$ of the total isotropic magnetic response M_{tot}^2 for different temperatures T. Solid lines are Lorentzian fits using Eq. (7).
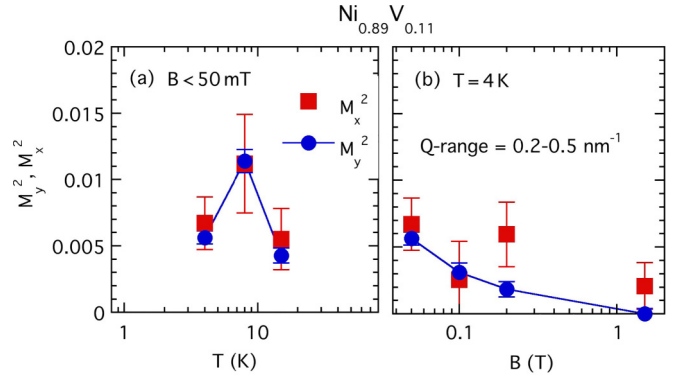

FIG. 8. Magnetic components M_y^2 and M_x^2 extracted from fit [Eq. (1)] of SF(θ) data (shown in Fig. 6) of Ni$_{0.89}$V$_{0.11}$ with $T_c \approx 7$ K at medium Q range of $(0.2$–$0.5)$ nm^{-1}. Panel (a) shows T dependence of isotropic fluctuations in small fields $(B \leqslant 50$ mT) and (b) shows B dependence of short-range correlations at low $T = 4$ K, which are different for transverse and longitudinal components. Lines just connect data points.

However, we can rule out similar short-range correlations in polycrystalline Ni samples (see in Sec. IV A).

The signature of a quantum Griffiths phase with a cluster distribution in FM Ni$_{1-x}$V$_x$ came from the field dependence of the bulk magnetization M [26]. The characteristic B dependence of $M(B)$ in the form of a power law indicates that these fluctuations of different sizes and rates are gradually freezing out toward higher B. The SANS data at low fields confirm already the existence of isotropic magnetic fluctuations at base T; SF data in higher magnetic fields should reveal more detailed information about the distribution. We notice in Fig. 6(b) already that the SF response and SF contrast M_y^2 at 4 K decrease in higher fields. The angle dependence also changes; it shows deviations from a pure sine-square form in higher B that indicates an anisotropic magnetic signal. The fit of Eq. (1) reveals different M_y^2 and M_x^2 components as presented in Fig. 8(b). The transverse component M_y^2 is decreasing with B while the longitudinal component M_x^2 does not change within large error bars. The Ni$_{0.90}$V$_{0.10}$ data [Figs. 3(a) and 3(b), Figs. 4(c) and 4(d)] support the same trend: M_y^2 decreases with B while M_x^2 remains finite. Both SF(θ) and NSF(θ) yield consistently a dominant M_x^2 component in high field. We did not expect to see a remaining magnetic longitudinal component M_x^2 at finite Q in strong magnetic fields. Since these SF data do not allow us to explore further the Q dependence of this term we postpone the discussion to the the next sections. In Secs. III C and III D we employ another method DIF that is better suited to resolve this anisotropic term.

We do understand and expect that M_y^2 decreases with B. That signals that the fluctuations indeed freeze out in higher field; more moments from short-range correlations do not contribute to this higher Q region since they might join larger domains. Unfortunately, we cannot resolve the detailed Q dependence and B dependence to find a specific cluster distribution. The statistics are too poor to even extract a Lorentzian fit with two parameters from $M_y^2(Q)$ in high fields that is further reduced compared to low fields. Fitting the
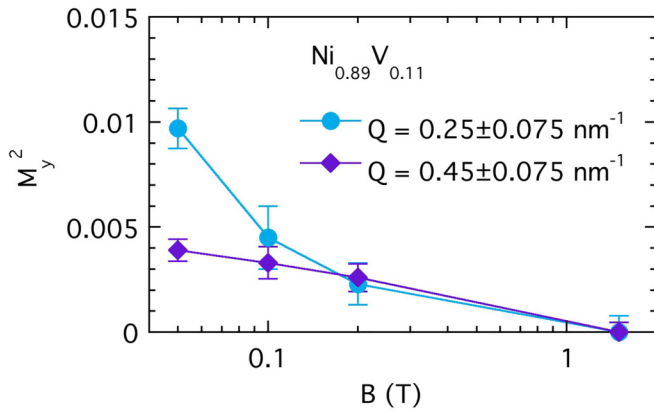
FIG. 9. Field dependence of magnetic component M_y^2 of $Ni_{0.89}V_{0.11}$ at low $T = 4$ K. M_y^2 values estimated from SF(θ) using Eq. (1) at two different Q ranges as indicated. Lines just connect data.

angle dependence of SF data collected in wide Q ranges of $\Delta Q = 0.15$ nm^{-1} provides sufficient statistics to trace $M_y^2(B)$ at two different Q locations. Figure 9 presents $M_y^2(B)$ for $Ni_{0.89}V_{0.11}$ obtained from SF(θ) at different Q, comparing a lower Q range (centered at 0.25 nm^{-1}) and a higher Q range (centered at 0.45 nm^{-1}). We notice that M_y^2 shows a steeper B dependence at lower Q than at higher Q. This trend is consistent with the idea that larger, slower clusters freeze out in smaller fields than smaller clusters with higher fluctuation rates. Our data might support a distribution of fluctuating cluster sizes consistent with quantum Griffiths singularities. Better resolution is certainly necessary to see and confirm more details.

C. Search for long-range order in $Ni_{0.90}V_{0.10}$

Another way to extract the longitudinal magnetic scattering is to consider the difference response DIF between the two initial polarization directions without analyzing the neutron polarization after the sample. The NSF asymmetry or flipper difference is collected from fully polarized data (DD-UU) or half-polarized (HP) data (D-U) as introduced before in Sec. II C, where Eq. (6) presents the characteristic angle dependence of DIF(θ). This interference term of nuclear and magnetic origin, $2NM_x$, more easily confirms a weak magnetic signal with a strong nuclear contribution. It is therefore accessible in a larger Q regime in $Ni_{1-x}V_x$ providing further information on different length scales than the fluctuations from the SF signal.

First we check the angular dependence of the DIF data in $Ni_{0.90}V_{0.10}$ for traces of a magnetic response in different Q regimes. Figure 10 shows DIF(θ) at low $T = 3$ K in $B = 0.2$ T for a low Q region (centered at $Q_{low} = 0.10$ nm^{-1}) in panel (a) and a high Q region (centered at $Q_{high} = 0.6$ nm^{-1}) in panel (b). The DIF(θ) data follow well the expected response of a sine-square function [see Eq. (6)] that confirms a longitudinal magnetic contribution M_x in the magnetized state. The maximum amplitude observed at DIF$(\theta = 90°) = $ DIFV $= 2NM_x$ is the only fit parameter. Figure 11 presents the detailed Q dependence of DIFV in a wide Q range from $Q = (0.06–1)$ nm^{-1}
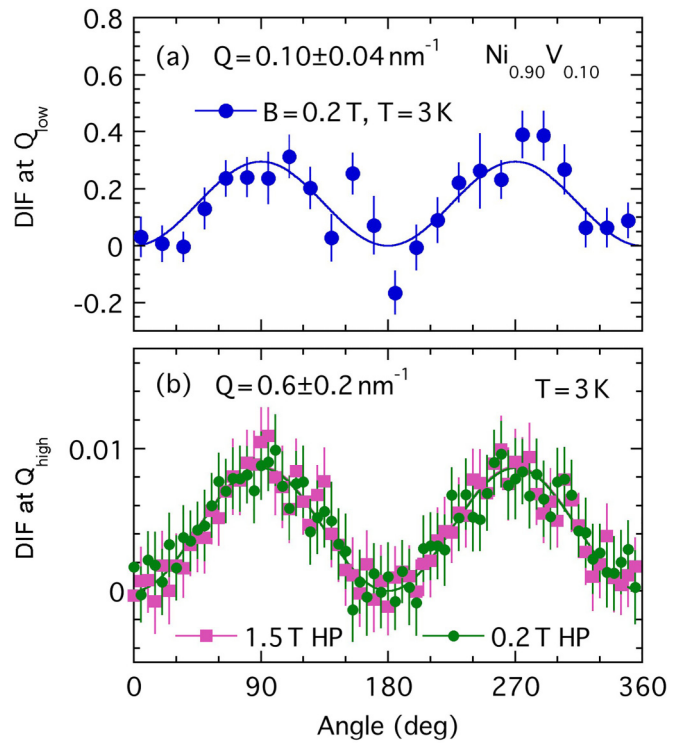

FIG. 10. Angle dependence of neutron response DIF(θ) of $Ni_{0.90}V_{0.10}$ for different Q ranges at low $T = 3$ K $< T_c$ confirming magnetic response $2NM_x$; solid lines follow Eq. (6). (a) Low Q range covers $(0.06–0.14)$ nm^{-1}; (b) high Q range includes $(0.4–0.8)$ nm^{-1}. HP denotes half-polarized data, where DIF $=$ D-U.

for $Ni_{0.90}V_{10}$ at base $T = 3$ K well below T_c. As long as the applied field is large enough ($B \geqslant 50$ mT) that the neutron beam does not become depolarized ($P_s > 85\%$) in the FM state of the sample, the DIFV(Q) response looks similar for different B. Toward low Q, the signal presents a steep $1/Q^n$ upturn that follows a "Porod" term [39] with power $n = 4$.
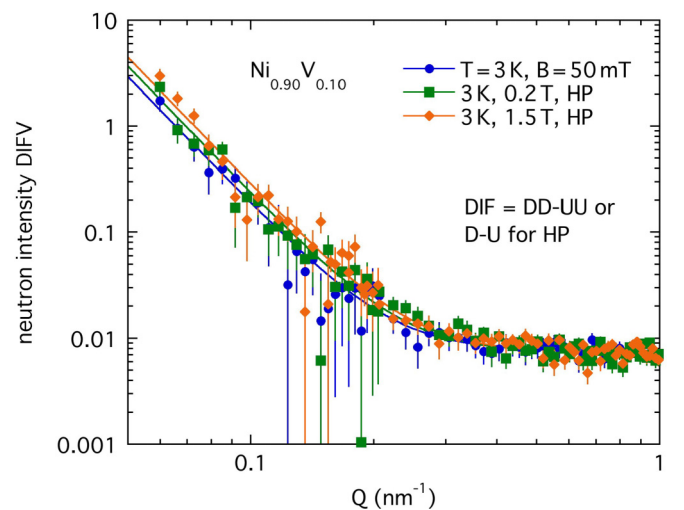

FIG. 11. Q dependence of DIFV $= 2NM_x$ of $Ni_{0.90}V_{0.10}$ at low $T = 3$ K $< T_c$ in magnetic fields B. Solid line indicates fit according to Eq. (8).
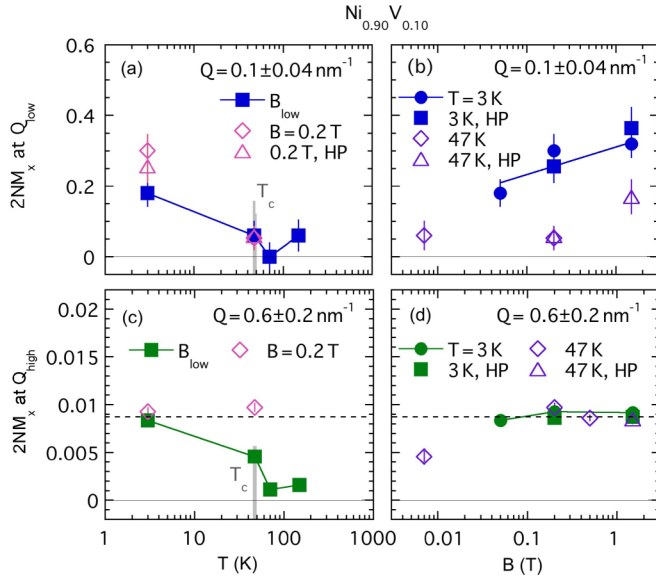
FIG. 12. Magnetic response $2NM_x$ of $Ni_{0.90}V_{0.10}$ for low Q [upper panels (a), (b)] and high Q [lower panels (c), (d)] derived from $DIF(\theta)$. The left panels [(a), (c)] compare the temperature dependence in small magnetic fields as indicated ($B_{low} \leqslant 50$ mT), the right panels [(b), (d)] the field dependence at $T = 3$ K $< T_c$ and $T = 47$ K $= T_c$. While $2NM_x$ at Q_{low} represents the long-range magnetic domain contribution, $2NM_x$ at Q_{high} signals local magnetic impurities. The solid lines connect data points in (a), (c), (d).

Toward higher Q the intensity remains constant. $DIF(Q)$ can be represented by

$$DIFV(Q) = A_D/Q^4 + C_D. \tag{8}$$

We recognize two different responses of aligned magnetic moments M_x in the B direction dominant at lower Q and remaining at higher Q in the FM state at 3 K. To distinguish their origin we study the evolution with T and B.

The upper panels of Figs. 12(a) and 12(b) focus on the interference term $2NM_x$ at Q_{low} representative of the low Q upturn with amplitude A_D. The $2NM_x(Q_{low})$ signal is present at the lowest temperature in fields $B \geqslant 50$ mT that can be analyzed in the FM state. As shown in panel (a) a clear positive response of $2NM_x$ appears only in the FM phase. $2NM_x$ becomes very small close to zero toward higher T when crossing the critical temperature $T_c = 47$ K into the PM state. The minor deviation from zero at higher T is not significant. The signal at low T is further increasing by applying a higher B as shown in panel (b). The field also changes the response in the PM regime at $T = 47$ K $\approx T_c$ but much less than in the ordered state below T_c. Further higher precision data at several T below and above T_c could trace and reveal the onset of a FM response in more detail. However, these changes in $2NM_x(T, B)$ are clearly related to the "magnetic" contribution M_x that appears below and vanishes above T_c.

As this mixed term $2NM_x$ includes the nuclear contribution, we check the pure nuclear contribution N^2 separately for any anomalies in T, B and in particular in Q to get a better estimate of the pure magnetic response. The pure nuclear signal from coherent scattering from Ni, N^2, is estimated from the total NSF contribution in a sector along the field

direction (NSFH = $N^2 + BG$) after other BG subtraction of mainly sample holder. $N^2(Q)$ shows a $1/Q^4$ dependence toward low Q (see Ref. [38]) without any obvious T or B dependence. This strong nuclear response in this lower Q range stems from grain boundaries of crystallites on the order of μm in these polycrystalline samples. The grain size is too large to be determined from these SANS data in this Q regime (1 μm $> 1/Q_{min} = 1/0.05$ nm^{-1}). Since the nuclear $N^2(Q)$ and the cross term $2NM_x(Q)$ exhibit a $1/Q^4$ dependence in the observed Q range, the magnetic term $(M_x)^2(Q)$ follows then also a $1/Q^4$ dependence from the simple estimate of $(M_x)^2 = (2NM_x)^2/(4N^2) \sim Q^{-4 \times 2}/Q^{-4} = Q^{-4}$. The precision of $2NM_x$ and M_x is far less than N^2 but deviations from $1/Q^4$ are not obvious. Therefore the Q dependence of $2NM_x(Q)$ does not contradict and rather might support large-scale magnetic domains of similar order to the grain sizes. This is in agreement with the simple depolarization estimates (see Appendix). The fact that the sample depolarizes the neutron beam strongly indicates FM order of large-scale domains on the order of μm. Lower Q data with better precision might increase the chance to notice deviations from power $n = 4$. This could reveal indication of a fractal nature of perforated domains [40] or reduced domain sizes. Recognizing saturation effects at lower Q might improve estimates of a domain size, e.g., assuming a simple Lorentzian-square fit [41]. So far, the lower limit is only 50 nm (see Ref. [38]). Note that, e.g., nanocrystalline Ni with average crystallite size of about 50 nm presents a different response [42]. $DIF(Q)$ is weakly Q-dependent [42]; it does not display the steep $1/Q^4$ upturn, or the constant Q term toward higher Q.

This DIFV signal at low Q in $Ni_{0.90}V_{0.10}$ shows the evolution of magnetic domains, long-range ordered regions, that develop below T_c. As we saw in the previous Sec. III A some short-range fluctuations remain at low T, but most of the Ni moments seem to form still a long-range ordered network in the FM state below T_c. We do not have evidence that the overall macroscopic domain size is reduced to short-range order or cluster freezing by the introduction of disorder through V in this alloy. As we see in Fig. 11 and Fig. 12 the upturn $2NM_x(Q_{low})$ still increases with B at low $T = 3$ K. At the same fields we notice that M_y^2 at higher Q range from SF is decreasing. While the short-range cluster fluctuations are freezing out, we expect that the contribution to the long-range magnetic domains are growing. Indeed, the data support consistently that the magnetic clusters freeze out gradually to join the ordered net moments that increase in field direction. Since the nuclear response does not show any anomaly at a magnetic transition, the response of $2NM_x(T, Q_{low})$ at low B marks the onset of FM order.

The second magnetic term in $2NM_x(Q)$ that becomes dominant at higher $Q > 0.2$ nm^{-1} is rather Q-independent within the investigated Q regime up to 1 nm^{-1}. The T and B dependence is different for this "high" Q term and points to a different origin than the low Q term. This constant C_D or $2NM_x(Q_{high})$ gradually decreases with increasing T without vanishing at T_c as shown in panel (c) of Fig. 12. Also, $2NM_x(Q_{high})$ does not change much with higher magnetic fields [see panel (d)]. It rather saturates at $2NM_x^{max}$ already in $B \geqslant 50$ mT for low and higher $T = T_c$, different than the low Q upturn that was related to long-range magnetic domains.

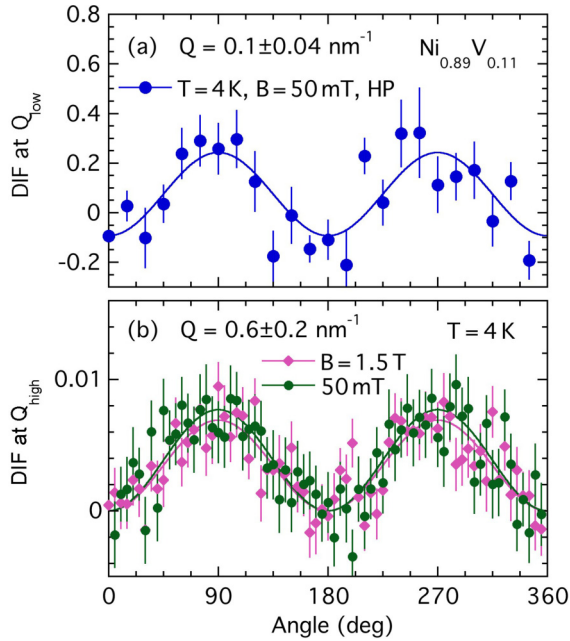FIG. 13. Angle dependence of DIF(θ) of $Ni_{0.89}V_{0.11}$ for different Q ranges at low $T = 4$ K $< T_c$ confirming magnetic response $2NM_x$; solid lines follow Eq. (6) with a small offset. (a) Low Q range covers (0.06–0.14) nm^{-1}; (b) high Q range includes (0.4–0.8) nm^{-1}. HP denotes half-polarized data, where DIF = D-U.

The Q independence supports that this high Q $2NM_x$ contribution stems from rather local defects in this $Ni_{0.90}V_{0.10}$ alloy. An extended Q range to larger Q is essential to probe the effective length scale of these defects. They become visible when the material is magnetized through entering the FM state forming domains or through an external magnetic field. We believe that this is not an instrumental artifact but a signature of defects introduced by the vanadium as we will show later in Sec. IV A through comparison with pure Ni data.

D. Search for long-range order in $Ni_{0.89}V_{0.11}$

Next, we explore the DIF response for the other concentration $x = 0.11$ closer to x_c. Also here we find signs of a longitudinal magnetic response M_x below T_c from the cross term $2NM_x$ in a large Q regime similar to $x = 0.10$. Figure 13 presents the characteristic angle variation of $\sin^2(\theta)$ in DIF(θ) [see Eq. (6)] at extreme Q regions, at $Q_{low} = 0.10 \pm 0.04$ nm^{-1} in panel (a) and at $Q_{high} = 0.6 \pm 0.2$ nm^{-1} in panel (b) at the lowest temperature $T = 4$ K for $B \geqslant 0.05$ T. Figure 14 shows then the Q dependence of the maximum response at DIFV at $T = 4$ K for $B \geqslant 50$ mT. It can be described by Eq. (8) by a $1/Q^4$ upturn and a remaining constant C_D similar to DIFV(Q) of $Ni_{0.90}V_{0.10}$. We see that this low Q scattering related to magnetic domains is increasing slightly with the magnetic field B, while the constant at high Q does not show any variation with the field. This extra DIFV = $2NM_x$ contribution at high Q confirms clearly a net magnetic M_x term that backs up the anisotropic component $M_x^2 > M_y^2$ from SF that persists in high fields as presented earlier in Fig. 8 in Sec. III B.
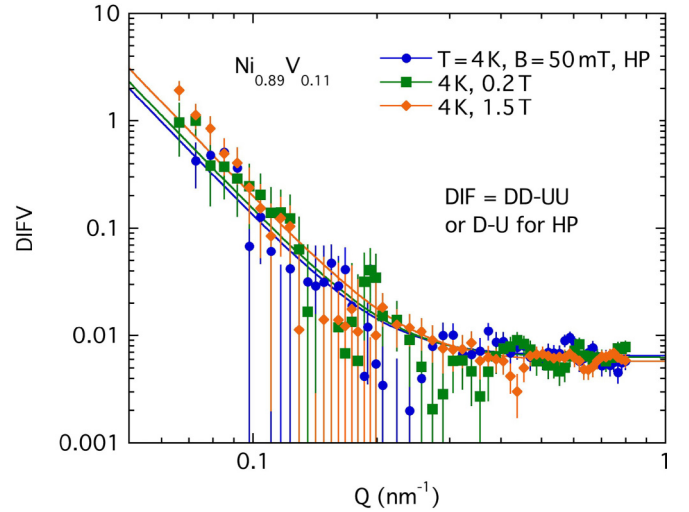

FIG. 14. Q dependence of DIFV = $2NM_x$ of $Ni_{0.89}V_{0.11}$ at low $T = 4$ K $< T_c$ in magnetic fields B. Solid line indicates fit according to Eq. (8).

This cross term DIFV that evaluates $2NM_x$ (derived from the difference of dominant nuclear responses) is of similar scale in $x = 0.11$ but shows more overall scatter than for $x = 0.10$. This is not surprising; we expect a smaller M_x (comparing $M(B)$ data [26]) and a larger N^2 for $Ni_{0.89}V_{0.11}$ than for $Ni_{0.90}V_{0.10}$. The $x = 0.10$ sample contains "natural" Ni, while the $x = 0.11$ sample is made from pure isotope ^{58}Ni with twice the coherent cross section of natural Ni. For $x = 0.11$ we take the maximum variation, the contrast between DIFV and DIFH, as the best $2NM_x$ estimate from DIF(θ). We accepted consistently for all runs a negative DIFH $= -0.18/ -0.12$ (polarized/HP) instead of ideally 0. This small deviation of $< 1\%$ of the large NSF signal seems within the resolution of the instrument and analysis. The parameter $2NM_x$ is evaluated for $x = 0.11$ for several temperatures and fields as shown in Fig. 15 for Q_{low} (upper panels) and Q_{high} (lower panels), similar to Fig. 12 for $x = 0.10$.

The low Q upturn in $2NM_x$ is represented through $2NM_x(Q_{low})$ in Figs. 15(a) and 15(b). It is present in the FM state at low T in magnetic fields ($B \geqslant 0.05$ T) that keep the beam sufficiently polarized. Panel (a) confirms that it develops only below T_c and marks the onset of FM order with long-range domains. The "precise" Q dependence for only $(M_x)^2(Q)$ cannot be revealed from DIFV(Q), but it does not contradict a $1/Q^4$ dependence without deviations due to long-range magnetic domains as explained for $Ni_{0.90}V_{0.10}$ above. Additional support for long-range ferromagnetic order comes from the fact that this $Ni_{0.89}V_{0.11}$ sample depolarizes the beam below T_c (see Appendix). A simple estimate from neutron depolarization suggests a domain size of few μm. Data toward lower Q with better statistics are necessary to clarify more details.

The amplitude of the low Q upturn recorded at low T, $2NM_x(Q_{low})$, is gradually growing in higher fields as shown in Fig. 15(b) and Fig. 14. Previously in Sec. III B we saw that the fluctuations M_y^2 at high Q decrease with B. This consistently supports the picture of short-range clusters joining larger domains. $Ni_{0.89}V_{0.11}$ shows similar magnetic signatures
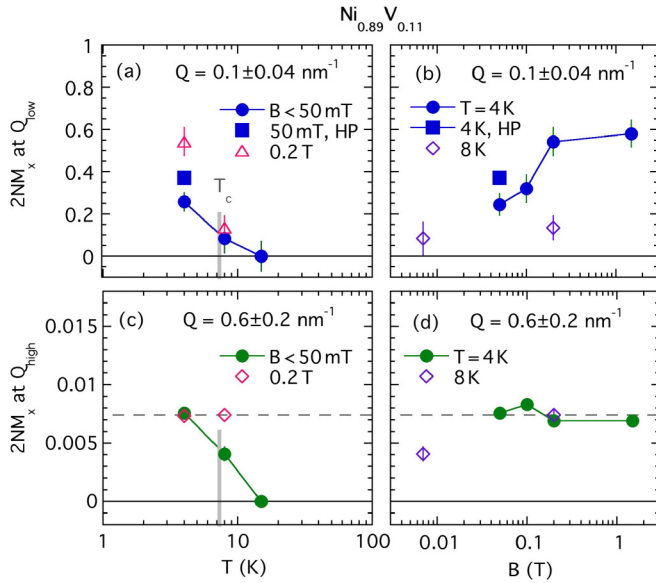
FIG. 15. Magnetic response $2NM_x$ of $Ni_{0.89}V_{0.11}$ for low Q [upper panels (a), (b)] and high Q [lower panels (c), (d)] derived from DIF(θ). The left panels [(a), (c)] compare the temperature dependence in small magnetic fields as indicated ($B_{low} \leqslant 50$ mT), the right panels [(b), (d)] the field dependence at $T = 4$ K $< T_c$ and $T = 8$ K $\approx T_c$. While $2NM_x(Q_{low})$ represents the ordered domain contribution, $2NM_x(Q_{high})$ stems from local magnetic impurities.

to $Ni_{0.90}V_{0.10}$, mainly that large-scale magnetic domains still form in the FM state although short-range magnetic fluctuations are becoming more dominant. The high Q DIF signal or remaining constant C_D represented by $2NM_x(Q_{high})$ is also present in $Ni_{0.89}V_{0.11}$. The lower panels [(c), (d)] of Fig. 15 show that it vanishes gradually with increasing temperature and saturates already in medium fields at any T. Similarly to $Ni_{0.90}V_{0.10}$ any external field or FM state is sufficient to magnetize the sample to notice these defects in $Ni_{0.89}V_{0.11}$.

The more diluted sample $Ni_{0.89}V_{0.11}$ follows the same trend of $Ni_{0.90}V_{0.10}$; the magnetic $2NM_x$ signal is essentially zero at temperatures above $T \geqslant T_c$ but appears below T_c. This indicates FM order within macroscopic domains even very close to the critical point. We collected three different magnetic responses in $Ni_{0.90}V_{0.10}$ and $Ni_{0.89}V_{0.11}$ through SF and DIF in different Q ranges. For both samples, we could extract short-range fluctuations remaining at low T but also find signatures of long-range domain scattering. To further check the origin and the importance for a disordered alloy we compare the signals with pure Ni and discuss the evolution with the vanadium dilution.

IV. DISCUSSION

A. SANS response of Ni vs Ni-V alloy

To clarify which magnetic effects are induced by vanadium, we compare the magnetic responses of the alloy $Ni_{0.90}V_{0.10}$ with pure Ni. Since $x = 0.11$ was made with ^{58}Ni, this sample cannot be used for this comparison. We performed a polarized SANS measurement at a different instrument, VSANS, for a Ni sample that was prepared with the same annealing protocol as the alloys. We covered a large Q range
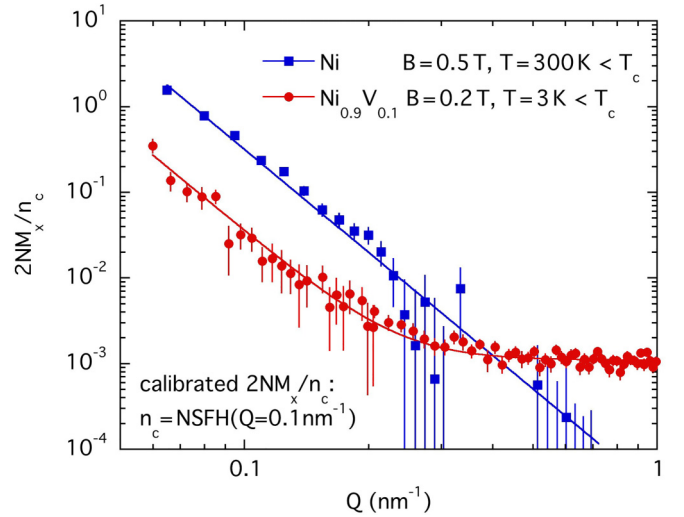

FIG. 16. Calibrated DIF response $2NM_x/n_c$ for Ni and $Ni_{0.90}V_{0.10}$ vs wave vector Q. In Ni only the long-range ordered domain term is present; the local defects appear in the V alloy. The solid line is fit according to Eq. (8).

at room temperature, 300 K, where Ni is in the ferromagnetic phase ($T_c = 630$ K). A stronger magnetic field of 0.5 T is needed for the Ni samples to avoid neutron beam depolarization. No clear net magnetic intensity results from the spin-flip contrast (SFH-SFV) with sufficient resolution that compares to the data of $x = 0.10$. The upper limit is well below the cluster contribution of the alloys. However, we resolve a significant magnetic response from the DIF term, the flipper contrast. To better compare the observed intensities of the alloy $Ni_{0.90}V_{0.10}$ and of Ni, measured under different conditions, we calibrate the signal with the nuclear scattering term at low Q. In both samples we expect the nuclear scattering to be dominated by the same (natural) Ni material with the same Ni coherent scattering. So we calibrate the observed intensity DIFV = $2NM_x$ by dividing through the observed nuclear response N^2. This signal is measured by NSFH (after BG correction using the empty sample holder). We use here the value of N^2 at $Q_{low} = 0.1$ nm^{-1} that is part of the $1/Q^4$ Porod term as calibration constant $n_c = N^2(Q_{low})$. The calibrated $2NM_x(Q)/n_c$ should then be independent of the spectrometer configuration and sample size.

Figure 16 compares the Q dependence of the calibrated DIF term, $2NM_x/n_c$, of $Ni_{0.90}V_{0.10}$ and Ni at the lowest possible fields. We see clearly for both samples at low Q a dominating term A_D/Q^4; the amplitude is higher in pure Ni than in $Ni_{0.90}V_{0.10}$. At high Q, $2NM_x/n_c$ in Ni dips below the signal in the alloy; the extra constant C_D term of the alloy [in Eq. (8)] seems missing in Ni. This supports that these local magnetic defects are caused by vanadium in $Ni_{0.90}V_{0.10}$ and not already present in Ni due to other structural defects or domain wall boundaries.

Figure 17 summarizes the magnetic cross term $2NM_x/n_c$ at Q_{low} at different V concentration x. For better comparison ratios are shown normalized to $x = 0$. We see that the two SANS data points follow well the bulk magnetization data from previous study [4]. $M(5$ T$)$ represents the magnetization at high fields and $M(0$ T$)$ the spontaneous magnetization, the
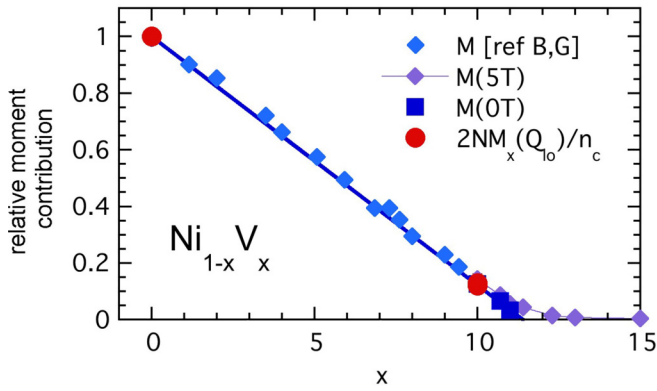
FIG. 17. Relative moment contribution vs vanadium concentration x from SANS results and other methods from Ref. [26]. $2NM_x(Q_{low})/n_c$ and bulk magnetization data $M(B)$ normalized to the value of Ni are shown. The long-range ordered domain term follows the trend of the linear reduction of the average magnetic moment with x.
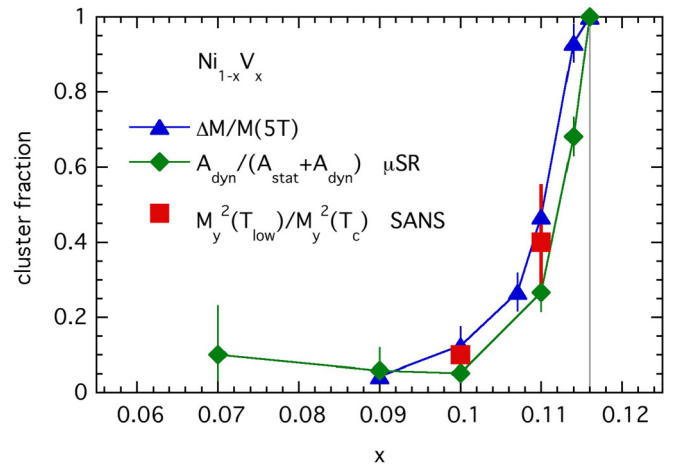

FIG. 18. Magnetic cluster fraction vs vanadium concentration x in $Ni_{1-x}V_x$ obtained from SANS compared to other methods: magnetization $M(B)$, μSR from Ref. [26]. The SANS estimate is the ratio of the SF contrast at lowest T and T_c, taken in medium Q range.

extrapolated value for 0 T. The slight magnetic field dependence does not affect much the ratio. (The ratio of the bulk moment estimate of $x = 0$ and $x = 0.1$ increases from 0.13 in $B = 0$ T to 0.14 in $B = 5$ T, while the $2NM_x/n_c$ ratio estimate is 0.12 in 0.2 T and 0.13 ± 0.02 in 1.5 T).

It is remarkable that the magnetic moment estimates from bulk data $M(B)$ and from SANS, extracting the Porod term $2NM_x(Q_{low})$, agree so well with each other. This DIF term does not only signal a magnetic response at low Q; it represents long-range ferromagnetic domain scattering. It even seems to measure the magnetic moment density and to function as an order parameter in this alloy. This cross term signal is so dominant since it is enhanced through the strong nuclear scattering of grain sizes in these polycrystalline samples. On one hand this is a huge "background" obstructing the SF scattering at the low Q range (that limits the precision of the magnetic short-range fluctuations); on the other hand this low Q upturn does provide useful information. This simple scaling and successful calibration also imply that the magnetic structure and crystalline structure of Ni do not change very much in the alloy Ni-V, at least in these samples with low V concentrations prepared with the same protocol. Not only the cross sections but also the domain and crystallite structure determine the small-angle scattering response. The Porod term with amplitude A_D typically depends on the contrast $(b_1 - b_2)^2$ of the scattering length densities b_1 and b_2 but also on the surface properties and area S in between the different scattering centers. Proper calibration with the nuclear term ($n_c = N^2$) assumes that the grain boundaries do not change much in the alloy compared to Ni. This agrees with a structural PDF analysis that notices minor defects in Ni but does not find changes in crystalline quality upon alloying [26,30]. The fact that the $2NM_x(Q_{low})/n_c$ terms scale as the spontaneous magnetization $M(0 \text{ T})$ term suggests that also the FM domain sizes and boundaries between FM domains and potential PM inclusion do not differ much in the diluted alloys and in pure Ni. Such structural and magnetic characterization is possible to extract from a simple cross term $DIFV(Q)$ that presents only one fit parameter: the amplitude of the Porod

term A_D. It works because Ni and $Ni_{0.90}V_{0.10}$ contain the same nuclear scattering centers (natural Ni) and magnetic scattering centers. The present data from the $Ni_{0.89}V_{0.11}$ samples made with the ^{58}Ni isotope cannot be easily used for this simple comparison. Further studies become necessary to study the domain scattering at higher vanadium concentration closer to x_c when the fluctuations become more dominant and the remaining ordered network weakens.

B. Evolution of magnetic clusters with disorder

The contribution of FM ordered moments measured by the domain term decreases with introducing vanadium into the alloy $Ni_{1-x}V_x$. At the same time some short-range magnetic fluctuations seem to develop in the FM state toward the critical V concentration x_c before the long-range order breaks down. We measure the magnetic cluster contribution by the leftover SF contrast at low T. To assess a cluster fraction we take the ratio of the signal intensity at lowest T and at $T \approx T_c$ where all moments should be still in the PM phase. Figure 18 shows the cluster fraction of the SANS measurement comparing with previous estimates from μSR and magnetization [26] as a function of x. The magnetization data define the power law increase in field up to 5 T as cluster contribution ΔM. The μSR analysis recognizes an additional dynamic term as paramagnetic cluster contribution besides a static term describing the FM response. All these estimates agree well within their precision confirming the evolution of increasing magnetic fluctuations breaking the FM order at $x_c = 0.116$. All data were taken at the lowest temperature of about 2 K. The present SANS data include data at 3 K and 4 K and nonpolarized data taken at 1.5 K. The cluster ratio for $x = 0.11$ is slightly T-dependent, but not vanishing. The error bar includes possible uncertainties due to low T extrapolations. A two-component picture of PM and FM contribution is certainly oversimplified, but the present new SANS data rectify that extreme scales of long-range domains and a short-range scale of few nm are relevant in this alloy. Generally, it is clear that disorder renders the exchange

interaction which ultimately leads to the emergence of the itinerant ferromagnetic state to become spatially inhomogeneous. As a result, one may expect that in a region of a sample, the local value of the exchange coupling would exceed the critical value of the averaged interaction constant leading to the formation of the ferromagnetic droplet. In two spatial dimensions, the size of the droplet does not depend on a size of the magnetic moment [43], while in the three-dimensional case this is not so. In either case, the dynamics of these droplets will be determined by the correlators of the randomly distributed coefficients in the Ginzburg-Landau functional. We leave the analysis of the magnetic susceptibility and heat capacity for future studies.

V. CONCLUSION

Although the average magnetic moment in $Ni_{1-x}V_x$ becomes very small close to the critical point where FM order vanishes, this SANS study identifies successfully magnetic scattering. The polarized SANS technique helps in particular to extract the small magnetic signal from the huge nuclear scattering. The pure spin-flip (SF) response and the flipper difference (DIF) reveal complementary magnetic contributions at various length scales in $Ni_{1-x}V_x$ close to critical concentration x_c where the onset of ferromagnetism at T_c extrapolates to zero. The two samples with vanadium concentration of $x = 0.10$ and $x = 0.11$ present similar responses in the accessible Q regime of $(0.06–0.1)$ nm^{-1} and are analyzed using simple forms. The result of a pure Ni sample serves as reference for a polycrystalline FM without atomic disorder.

First, we confirm the presence of magnetic clusters at the lowest temperatures far below T_c. The angular and Q dependence (of the SF response) reveal isotropic magnetic short-range correlations similar to the paramagnetic fluctuations seen close to T_c. The scale of these correlations is 5–10 nm estimated by a simple Lorentzian function. These fluctuations get suppressed gradually in higher fields and follow qualitatively the expectations of the quantum Griffiths phase where magnetic clusters freeze with different fluctuations rates. The SF data give an estimate of the fraction of these magnetic clusters that do not contribute to the magnetic order. The cluster ratio is determined through the remaining few clusters at low T in the FM phase compared to the PM signal close to T_c. This cluster contribution increases significantly from $x = 0.10$ to $x = 0.11$, demonstrating that these short-range correlated fluctuations become more important toward x_c. The new SANS data agree well with previous cluster estimates from magnetization and μSR data [26] supporting further the different dynamics of these contributions.

In addition, we find signatures of long-range domain scattering, which supports macroscopic long-range order for samples even very close to x_c. Within this Q range we cannot measure the macroscopic length scale, but only set lower limits and collect supporting evidence. The neutron beam gets depolarized below T_c for both samples. The magnetic cross term $DIF = 2NM_x$ shows a low Q upturn due to long-range domain scattering with aligned moments M_x similar to the pure nuclear scattering term N^2 due to grain boundary scattering. This low Q magnetic domain term only appears below T_c and is field-dependent. In higher magnetic fields, the low Q

domain term increases while the medium Q fluctuation term decreases, indicating that the short-range fluctuations freeze to join the larger domains with aligned moments. A comparison with Ni even shows that this low Q contribution scales with the magnetic moment estimates from bulk magnetization measurements. So, this low Q domain term not only confirms long-range order but also reveals the ordered moment of the compound.

These SANS data provide remarkable information although the individual data lack precision in resolving details of a system with moments of less than 0.1 μ_B/Ni. We see clear evidence of various magnetic correlations in this alloy produced by random atomic dilution. We notice correlation lengths from nm scale to μm employing simple tools. These various contributions confirm that the FM order does not get homogeneously destroyed. On the other hand we do not notice any signs of a spin glass or cluster glass with only frozen short-range correlations. We do not see macroscopic phase separation either of different ordered phases. Note that a SANS response with a Porod or Lorentzian square term indicating longer-range domains and a shorter-range Lorentzian term is often observed in alloys and transition metals oxides (see, e.g., in Ref [20]). Typically, the size of the long-range order is already limited [41] or gets reduced by chemical substitution before the magnetic order breaks down [44]. The two coexisting phases are expected to both be magnetic ordered phases with relevant coercivity [45]. We come to a different conclusion in our simple d-metal alloy $Ni_{1-x}V_x$ with sustained long-range order and coexisting fluctuations close to x_c. Our prepared samples remain a soft metal and do not show any hysteresis in $M(B)$ [4]. The SANS data reveal macroscopic domains that are unavoidable in a finite-sized soft FM. We fit only two contributions of FM domains and PM clusters to facilitate a description of a variety of length and time scales present in these samples. It is likely that through quenched disorder the correlated regions vary throughout the alloy, leading to a network of longer-range domains that are perforated by shorter-range fluctuations (provoked by the random location of the V atoms). This disorder can lead to a quantum critical point in a FM metal. Here we tried to measure a typical scale of short-range correlations that stems from a distribution. We cannot see the local arrangement or a pattern formation. A complimentary method with spatial resolution in nm would be of high interest to perform in order to reveal the location, distribution, and shape of clusters and of coexisting long-range domains. This simple model system $Ni_{1-x}V_x$ with controlled random atomic distribution offers a great opportunity to study the complex interaction of a d metal with short- and long-range interaction including local random defects. The present SANS data allow insight in the mechanism of how fluctuations evolve in the FM ordered state that lead to a quantum critical point in an itinerant FM.

APPENDIX: NEUTRON DEPOLARIZATION

The main study concentrates on the "scattered" neutron intensities from the magnetic sample using the different cross sections with selected neutron polarization. The polarizing devices such as the supermirrors, spin flipper, and ^{3}He spin filter, where the polarizing efficiency decays with time, are certainly not perfect and do not produce a 100% polarized beam. Collecting the transmitted direct beam intensity for all 4 spin combinations gives typically sufficient information for correction of such spin leakage. Another source for the depolarization of the neutron beam is the magnetic sample. On one hand depolarization measurements provide important information [46–48]; they can help to diagnose the magnetic state of the sample in particular for ferromagnets [49,50]. On the other hand a strong depolarization mixes and affects the different scattered intensities of the 4 cross sections that might make a proper polarization analysis unresolvable [51]. The polarization state P_S of the transmitted neutron beam due to the sample is essentially measured by the contrast of transmitted direct beam without spin flip T_{NSF} and with spin flip T_{SF} (for perfect polarizing devices with initial $P_0 = 1$):

$$P_s = [T_{NSF} - T_{SF}]/[T_{NSF} + T_{SF}]. \quad (A1)$$

P_s remains 1, when no change in the initial spin direction occurs. Conversely, P_s goes down to 0, when the neutron spin loses completely its original orientation that the intensity of both initial and reversed direction are equal.

To check if the Ni-V samples depolarize the neutron beam and to find optimized working conditions to collect polarized scattering data we recorded the transmitted neutron beam polarization P_s from the (efficiency corrected) transmission data at different temperature T and magnetic fields B. Figure 19 presents P_s for alloys with $x = 0.10$ and $x = 0.11$. P_s is close to 1 for high temperatures in the paramagnetic region, but starts declining below the critical temperature T_c. Both samples are clearly depolarizing the beam in a small field of 7 mT. For $x = 0.10$ P_s saturates at low T at a small value of
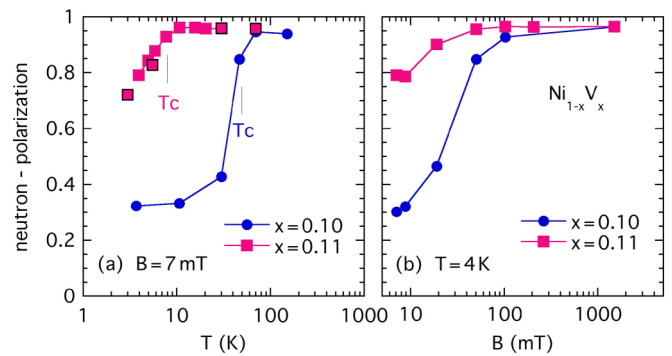

FIG. 19. Transmitted neutron beam polarization ratio P_s of the sample ($Ni_{0.90}V_{0.10}$ and $Ni_{0.89}V_{0.11}$) at different environments. Panel (a) presents the temperature T dependence in a small field; both samples depolarize the beam for $T < T_c$. Panel (b) shows how the polarization recovers in applied magnetic fields B at a low temperature.

$P_s = 0.3$; for $x = 0.11$ P_s reaches 0.7 at 3 K. As expected the strong depolarization changes in higher fields. At a magnetic field of 1 T, the maximum value close to 1 is recovered; at 50 mT P_s increases to 0.85 for $x = 0.10$. We conclude that low T scattering data taken at 50 mT show sufficient polarization for $Ni_{1-x}V_x$ with $x \geqslant 0.10$.

Neutron depolarization is caused by strong internal fields that change on a mesoscopic scale. The different field directions make the neutron spin precess and deviate from the main polarization direction. Local defects or fast fluctuations in the sample do not affect the spin, but differently oriented long-range domains in a soft ferromagnet is the typical case that leads to depolarization as we are suspecting here. When these magnetic domains align in higher magnetic fields, the neutron polarization gets restored. The observed values of P_s depend on the strength of the inner fields and the neutron time spent precessing to reach an effective precession angle ϕ and therefore on the dimensions the domain size δ and the sample thickness d. We use a simple model proposed in Ref. [49] to estimate a typical domain size from P_s:

$$P_s = P_f/P_i = \exp\left(-\frac{d}{3\delta}\phi_\delta^2\right), \quad (A2)$$

where P_f and P_i are the final and initial neutron beam polarization. The precession angle $\phi_\delta = (4.63 \times 10^{-10} \, G^{-1} \, Å^{-2})\lambda B\delta$ depends on neutron wavelength λ, magnetic field B, and the domain size δ. $B = 4\pi M_s \rho$ can be estimated from spontaneous magnetization M_s with density ρ (all expressions in cgs units [49]). For $x = 0.10$ and $x = 0.11$ we find $B = 810$ G and $B = 190$ G from the magnetization data [26], which yield domain sizes of 3 μm and 2 μm, respectively. This estimate of similar domain sizes is certainly too crude for the present alloys, but these depolarization data demonstrate that both samples show all indications of ferromagnetic order at low $T < T_c$ with long-range domains on the order of μm.

[1] E. C. Stoner, Collective electron ferromagnetism, Proc. R. Soc. London A **165**, 372 (1938).

[2] E. C. Stoner, Ferromagnetism, Rep. Prog. Phys. **11**, 43 (1947).

[3] I. Y. Pomeranchuk, On the stability of a Fermi liquid, Sov. Phys. JETP **8**, 361 (1959).

[4] S. Ubaid-Kassis, T. Vojta, and A. Schroeder, Quantum Griffiths Phase in the Weak Itinerant Ferromagnetic Alloy Ni$_{1-x}$V$_x$, Phys. Rev. Lett. **104**, 066402 (2010).

[5] S. Sachdev, *Quantum Phase Transitions* (Cambridge University Press, Cambridge, 2011).

[6] T. Vojta and J. A. Hoyos, Criticality and Quenched Disorder: Harris Criterion Versus Rare Regions, Phys. Rev. Lett. **112**, 075702 (2014).

[7] T. Vojta, Rare region effects at classical, quantum and nonequilibrium phase transitions, J. Phys. A: Math. Gen. **39**, R143 (2006).

[8] T. Vojta, Phases and phase transitions in disordered quantum systems, AIP Conf. Proc. **1550**, 188 (2013).

[9] T. Vojta, Quantum Griffiths effects and smeared phase transitions in metals: Theory and experiment, J. Low Temp. Phys. **161**, 299 (2010).

[10] G. R. Stewart, Non-Fermi-liquid behavior in *d*- and *f*-electron metals, Rev. Mod. Phys. **73**, 797 (2001).

[11] K. Huang, S. Eley, P. F. S. Rosa, L. Civale, E. D. Bauer, R. E. Baumbach, M. B. Maple, and M. Janoschek, Quantum Critical Scaling in the Disordered Itinerant Ferromagnet UCo$_{1-x}$Fe$_x$Ge, Phys. Rev. Lett. **117**, 237202 (2016).

[12] B. C. Sales, K. Jin, H. Bei, J. Nichols, M. F. Chisholm, A. F. May, N. P. Butch, A. D. Christianson, and M. A. McGuire, Quantum critical behavior in the asymptotic limit of high disorder in the medium entropy alloy NiCoCr$_{0.8}$, npj Quantum Mater. **2**, 33 (2017).

[13] A. K. Mishra, S. Shanmukharao Samatham, M. R. Lees, and V. Ganesan, Disorder-induced critical exponents near a ferromagnetic quantum critical point in Mn$_{1-x}$Cr$_x$Si, Phys. Rev. B **101**, 144436 (2020).

[14] T. R. Kirkpatrick and D. Belitz, Exponent relations at quantum phase transitions with applications to metallic quantum ferromagnets, Phys. Rev. B **91**, 214407 (2015).

[15] M. Brando, D. Belitz, F. M. Grosche, and T. R. Kirkpatrick, Metallic quantum ferromagnets, Rev. Mod. Phys. **88**, 025006 (2016).

[16] T. R. Kirkpatrick and D. Belitz, Ferromagnetic Quantum Critical Point in Noncentrosymmetric Systems, Phys. Rev. Lett. **124**, 147201 (2020).

[17] C.-L. Huang, A. M. Hallas, K. Grube, S. Kuntz, B. Spieß, K. Bayliff, T. Besara, T. Siegrist, Y. Cai, J. Beare, G. M. Luke, and E. Morosan, Quantum Critical Point in the Itinerant Ferromagnet Ni$_{1-x}$Rh$_x$, Phys. Rev. Lett. **124**, 117203 (2020).

[18] B. Shen, Y. Zhang, Y. Komijani, M. Nicklas, R. Borth, A. Wang, Y. Chen, Z. Nie, R. Li, X. Lu, H. Lee, M. Smidman, F. Steglich, P. Coleman, and H. Yuan, Strange-metal behaviour in a pure ferromagnetic Kondo lattice, Nature (London) **579**, 51 (2020).

[19] J. W. Shu, D. T. Adroja, A. D. Hillier, Y. J. Zhang, Y. X. Chen, B. Shen, F. Orlandi, H. C. Walker, Y. Liu, C. Cao, F. Steglich, H. Q. Yuan, and M. Smidman, Magnetic order and crystalline electric field excitations of the quantum critical heavy-fermion ferromagnet CeRh$_6$Ge$_4$, Phys. Rev. B **104**, L140411 (2021).

[20] S. Mühlbauer, D. Honecker, E. A. Périgo, F. Bergner, S. Disch, A. Heinemann, S. Erokhin, D. Berkov, C. Leighton, M. R. Eskildsen, and A. Michels, Magnetic small-angle neutron scattering, Rev. Mod. Phys. **91**, 015004 (2019).

[21] M. F. Collins, *Magnetic Critical Scattering* (Oxford University Press, New York, 1989).

[22] A. P. Murani, P. Radhakrishna, K. Ibel, G. Goeltz, F. Mezei, S. Roth, B. D. Rainford, and B. R. Coles, Small angle critical neutron scattering and the onset of ferromagnetism in Au-Fe alloys, J. Phys. F **6**, 425 (1976).

[23] B. H. Verbeek, G. J. Nieuwenhuys, J. A. Mydosh, C. van Dijk, and B. D. Rainford, Inhomogeneous ferromagnetic ordering in PdFe and PdMn alloys studied via small-angle neutron scattering, Phys. Rev. B **22**, 5426 (1980).

[24] S. K. Burke and B. D. Rainford, The evolution of magnetic order in CrFe alloys. III. Ferromagnetism close to the critical concentration, J. Phys. F **13**, 471 (1983).

[25] S. V. Grigoriev, S. A. Klimko, W. H. Kraan, S. V. Maleyev, A. I. Okorokov, M. T. Rekveldt, and V. V. Runov, Magnetic phase transition in disordered Fe-Ni alloys studied by means of small-angle neutron scattering and three-dimensional analysis of the neutron depolarization, Phys. Rev. B **64**, 094426 (2001).

[26] R. Wang, A. Gebretsadik, S. Ubaid-Kassis, A. Schroeder, T. Vojta, P. J. Baker, F. L. Pratt, S. J. Blundell, T. Lancaster, I. Franke, J. S. Möller, and K. Page, Quantum Griffiths Phase Inside the Ferromagnetic Phase of Ni$_{1-x}$V$_x$, Phys. Rev. Lett. **118**, 267202 (2017).

[27] M. F. Collins and G. G. Low, The magnetic moment distribution around transition element impurities in iron and nickel, Proc. Phys. Soc. **86**, 535 (1965).

[28] J. Friedel, Metallic alloys, Nuovo Cim. **7**, 287 (1958).

[29] A. Schroeder, R. Wang, P. J. Baker, F. L. Pratt, S. J. Blundell, T. Lancaster, I. Franke, and J. S. Möller, Probing the magnetic phases in the Ni-V alloy close to the disordered ferromagnetic quantum critical point with μSR, J. Phys.: Conf. Ser. **551**, 012003 (2014).

[30] A. Gebretsadik, R. Wang, A. Alyami, H. Adawi, J.-G. Lussier, K. Page, and A. Schroeder, Study of atomic disorder in Ni-V alloys, arXiv:2302.01986.

[31] C. J. Glinka, J. G. Barker, B. Hammouda, S. Krueger, J. J. Moyer, and W. J. Orts, The 30 m small-angle neutron scattering instruments at the National Institute of Standards and Technology, J. Appl. Crystallogr. **31**, 430 (1998).

[32] J. Barker, J. Moyer, S. Kline, G. Jensen, J. Cook, C. Gagnon, E. Kelley, J. P. Chabot, N. Maliszewskyj, C. Parikh, W. Chen, R. P. Murphy, and C. Glinka, The very small angle neutron scattering instrument at the National Institute of Standards and Technology, J. Appl. Crystallogr. **55**, 271 (2022).

[33] K. Krycka, R. Booth, J. Borchers, W. Chen, C. Conlon, T. Gentile, C. Hogg, Y. Ijiri, M. Laver, B. Maranville, S. Majetich, J. Rhyne, and S. Watson, Resolving 3d magnetism in nanoparticles using polarization analyzed SANS, Phys. B: Condens. Matter **404**, 2561 (2009).

[34] W. Chen, R. Erwin, J. McIver III, S. Watson, C. Fu, T. Gentile, J. Borchers, J. Lynn, and G. Jones, Applications of ^{3}He neutron spin filters at the NCNR, Phys. B: Condens. Matter **404**, 2663 (2009).

[35] S. R. Kline, Reduction and analysis of SANS and USANS data using IGOR Pro, J. Appl. Crystallogr. **39**, 895 (2006).

[36] K. Krycka, W. Chen, J. Borchers, B. Maranville, and S. Watson, Polarization-analyzed small-angle neutron scattering. I. Polarized data reduction using Pol-Corr, J. Appl. Crystallogr. **45**, 546 (2012).

[37] R. M. Moon, T. Riste, and W. C. Koehler, Polarization analysis of thermal-neutron scattering, Phys. Rev. **181**, 920 (1969).

[38] A. Schroeder, S. Bhattarai, A. Gebretsadik, H. Adawi, J.-G. Lussier, and K. L. Krycka, Magnetic correlations in the disordered ferromagnetic alloy Ni-V revealed with small angle neutron scattering, AIP Adv. **10**, 015036 (2020).

[39] S. K. Sinha, E. B. Sirota, S. Garoff, and H. B. Stanley, X-ray and neutron scattering from rough surfaces, Phys. Rev. B **38**, 2297 (1988).

[40] A. Kreyssig, R. Prozorov, C. D. Dewhurst, P. C. Canfield, R. W. McCallum, and A. I. Goldman, Probing Fractal Magnetic Domains on Multiple Length Scales in $Nd_2Fe_{14}B$, Phys. Rev. Lett. **102**, 047204 (2009).

[41] F. Hellman, A. L. Shapiro, E. N. Abarra, R. A. Robinson, R. P. Hjelm, P. A. Seeger, J. J. Rhyne, and J. I. Suzuki, Long ferromagnetic correlation length in amorphous $TbFe_2$, Phys. Rev. B **59**, 11408 (1999).

[42] J. Weissmüller, A. Michels, J. G. Barker, A. Wiedenmann, U. Erb, and R. D. Shull, Analysis of the small-angle neutron scattering of nanocrystalline ferromagnets using a micromagnetics model, Phys. Rev. B **63**, 214414 (2001).

[43] B. N. Narozhny, I. L. Aleiner, and A. I. Larkin, Magnetic fluctuations in two-dimensional metals close to the Stoner instability, Phys. Rev. B **62**, 14898 (2000).

[44] J. M. De Teresa, C. Ritter, P. A. Algarabel, S. M. Yusuf, J. Blasco, A. Kumar, C. Marquina, and M. R. Ibarra, Detailed neutron study of the crossover from long-range to short-range magnetic ordering in $(Nd_{1-x}Tb_x)_{0.55}Sr_{0.45}MnO_3$ manganites, Phys. Rev. B **74**, 224442 (2006).

[45] S. El-Khatib, S. Bose, C. He, J. Kuplic, M. Laver, J. A. Borchers, Q. Huang, J. W. Lynn, J. F. Mitchell, and C. Leighton, Spontaneous formation of an exchange-spring composite via magnetic phase separation in $Pr_{1-x}Ca_xCoO_3$, Phys. Rev. B **82**, 100411(R) (2010).

[46] O. Halpern and T. Holstein, On the passage of neutrons through ferromagnets, Phys. Rev. **59**, 960 (1941).

[47] M. T. Rekveldt, Study of ferromagnetic bulk domains by neutron depolarization in three dimensions, Z. Phys. **259**, 391 (1973).

[48] S. Mitsuda and Y. Endoh, Neutron depolarization studies on magnetization process using pulsed polarized neutrons, J. Phys. Soc. Jpn. **54**, 1570 (1985).

[49] S. M. Yusuf, M. Sahana, M. S. Hegde, K. Dörr, and K.-H. Müller, Evidence of ferromagnetic domains in the $La_{0.67}Ca_{0.33}Mn_{0.9}Fe_{0.1}O_3$ perovskite, Phys. Rev. B **62**, 1118 (2000).

[50] I. Mirebeau, S. Itoh, S. Mitsuda, T. Watanabe, Y. Endoh, M. Hennion, and P. Calmettes, Evidence of magnetic domains in the reentrant spin glasses $Ni_{1-x}Mn_x$ studied by neutron depolarization, Phys. Rev. B **44**, 5120 (1991).

[51] Y. Quan, J. Steiner, V. Ukleev, J. Kohlbrecher, A. Vorobiev, and P. Hautle, Impact of the neutron-depolarization effect on polarized neutron scattering in ferromagnets, IUCrJ **8**, 455 (2021).